Springer

KSME

Journal of Mechanical Science and Technology 24 (5) (2010) 1119~1125
www.springerlink.com/content/1738-494x
DOI 10.1007/s12206-010-0304-9

Effects of structural configuration on vibration control of smart laminated beams under random excitations †

Abolghassem Zabihollah*

School of Science and Engineering, Sharif University of Technology, International Campus, Kish Island, Iran

(Manuscript Received September 4, 2009; Revised November 1, 2009; Accepted February 8, 2010)

Abstract

The influence of structural configuration on vibration responses of smart laminated beams under random loading is studied. The effect of laminate configurations and locations of sensors/actuators in the smart system is also investigated. The layer-wise approximation for displacement and electric potential is utilized to construct the finite element model. The closed-loop control response is determined through an optimal control algorithm based on the Linear Quadratic Regulator (LQR). The correlation coefficient between the input random force and the applied actuating voltage for various configurations is also computed. It is revealed that for softer configurations, the correlation coefficient is higher than that for harder configurations. The study on the effect of sensor/actuator collocation pairs on optimal vibration control reveals that as the actuator shifts away from the sensor location, the peak of power occurs at higher frequency and becomes more distributed through all the frequencies in the domain.

Keywords: Beams; Laminated; Layer-wise; Optimal control; Random; Smart; Vibration

1. Introduction

Laminated composite structures are often exposed to randomly varying dynamic loading, such as aircraft components (e.g., turbulence, acoustic pressure, or rough burning engines) and marine structures in which the variation of such a loading cannot be determined exactly. Studies on environmental excitations have resulted in questions on the response behavior. Excessive vibration in smart laminated structures may result in instability and/or poor functionality of the system. Therefore, it is critically important to control the response of the structure under random external loading. An appropriate mechanism for vibration control of such structures can be achieved mainly by considering the three most important factors: modeling of the laminate, control strategy, and performance under different loading, including random excitation.

To date, the majority of works on random vibration control of smart laminated composite structures utilized Equivalent Single Layer theories (ESL), including Classical Laminate Theory (CLT) [1], and the First-order Shear Deformation Theory (FSDT) by Librescu and Elishakoff [2] and Cederbaum et al. [3]. In an attempt to enhance the accuracy of the vibration response, Kang and Harichandran [4] developed a higher-order shear deformation formulation to analyze the vibration response of a laminated plate under random loading. Most recently, Dash and Singh [5] presented a nonlinear vibration control of a laminated composite based on FSDT.

The efficiency and accuracy of the dynamic response, and thus the control mechanism of smart laminates, highly depend on the structural modeling of the structure, loading conditions, and structural configurations. Layer-wise displacement theory can provide an accurate and efficient model for the vibration analysis of laminated structures [6]. The present author and colleagues [7] provided a comparison between the ESL theories and the layer-wise theory on the vibration control of smart-laminated beams. In designing an optimal control mechanism, Linear Quadratic Regulator (LQR) is an efficient approach to determine the optimal feedback gain. Optimal control based on LQR has been applied for the vibration control of many isotropic structures [8, 9]. Vasques and Rodrigues [10] provided a complete comparison between various control strategies for piezo-laminated beams with metallic core. Most recently, Levent [11] studied the effects of laminate configuration on the free vibration of laminated structures integrated with a piezoelectric actuator using a 3D finite element approach. It was found that the existence of different materials (e.g., sensor, actuator and composite, adhesive, etc.) in a typical smart laminate caused strong inhomogenieties through the thickness of the structure. Furthermore, structural configuration greatly influenced the dynamic response of the

† This paper was recommended for publication in revised form by Associate Editor Eung-Soo Shin

*Corresponding author. Tel.: +98 764 442299/351, Fax.: +98 764 4422828
E-mail address: zabihollah@sharif.edu

structures under random excitation. No other studies have discussed the issue of material inhomogenieties and structural configurations in random vibration control using the layer-wise displacement approximation and LQR controller. The present work aims to address this issue and to improve the existing knowledge on the design of smart laminated structures for aerospace applications.

2. Structural modeling

The displacement and electric potential fields in the laminated beam based on the layer-wise theory are given by

$$u(x,z,t)=\sum_{i}^{n}\sum_{j}^{m} U_{ij}(x,t)\Phi_i(z)\varphi_j(x)\,, \qquad (1)$$
$$\psi_1(x,t)=\psi_1^o(t)\,,\quad w(x,z,t)=W_o(x,t)\,,$$

where u is the displacement along x, ψ is the electrical potential, and n and m are the total number of nodes through the thickness and along the length, respectively. Interpolation functions $\Phi_i(z)$ and $\varphi_j(x)$ are defined along the z and x directions, respectively. The finite element model for a smart laminated beam based on the layer-wise approximation for displacements and electric potential can be obtained as [7].

$$\begin{bmatrix}[M_{dd}] & [0]\\ [0] & [0]\end{bmatrix}\begin{Bmatrix}\{\ddot{d}\}\\ \{\ddot{\psi}^s\}\end{Bmatrix}+\begin{bmatrix}[K_{dd}] & [K_{d\psi}^{ss}]\\ [K_{\psi d}^{ss}] & [K_{\psi\psi}^{ss}]\end{bmatrix}\begin{Bmatrix}\{d\}\\ \{\psi^s\}\end{Bmatrix}=\begin{Bmatrix}\{F_d(t)\}-[K_{d\psi}^{sa}]\{\psi^a\}\\ \{Q^s(t)\}-[K_{\psi\psi}^{sa}]\{\psi^a\}\end{Bmatrix} \qquad (2)$$

where $[K_{dd}]$, $[K_{d\psi}]$, $[K_{\psi\psi}]$, and $[M_{dd}]$ denote the elastic, piezoelectric, and permittivity matrices, and the mass matrix, respectively, and $\{F_d\}$ and $\{Q^s\}$ are the applied mechanical load and electrical charge vectors, respectively. The displacement $\{d\}=\{U\quad W\}^T$ represents a vector containing axial and transverse displacements, ψ^s denotes the voltage output at the sensor, and ψ^a is the voltage imposed on the actuator layer. Eq. (2) can also be reduced to the following independent equations to determine the generated voltage at the sensor as

$$\{\psi^s\}=-[K_{\psi\psi}^{ss}]^{-1}\left([K_{\psi d}^{ss}]\{d\}+[K_{\psi\psi}^{sa}]\{\psi^a\}\right), \qquad (3)$$

while the structural displacements are

$$[M_{dd}]\{\ddot{d}\}+[C]\{\dot{d}\}+[\hat{K}]\{D\}=\{F_d\}+[K_{d\psi}^{sa}]\{\psi^a\}\,, \qquad (4)$$

where $[\hat{K}]=[K_{dd}]-[K_{\psi d}^{ss}][K_{\psi\psi}^{ss}]^{-1}[K_{\psi d}^{ss}]$, $\{F_d(t)\}$ represents the external force vector generating the primary excitation, $\{\psi^a(t)\}$ is the control force applied to the system, and $[K_{d\psi}^{sa}]$ defines the location of the actuators as well as converts the applied electric field to the mechanical force. The coefficients of element matrices are provided in the Appendix.

3. Random vibration analysis

In vibration control, designing a control algorithm to direct specific modes of vibrations is more practical. Using the mode superposition method $\{d(t)\}=[q]\{\eta(t)\}$, the modal form of Eq. (4) can be expressed as [4]

$$[I]\{\ddot{\eta}(t)\}+[D]\{\dot{\eta}(t)\}+[\Omega]\{\eta(t)\}=[q]^T\{F_d(t)\}+[q]^T[K_{d\psi}^{sa}]\{\psi^a(t)\} \qquad (5)$$

The power spectral density matrix of the displacement response $[S_\eta(\omega)]$ is given by [12]:

$$[S_\eta(\omega)]=[H_\eta(\omega)][S_P(\omega)][H_\eta^*(\omega)]^T\,, \qquad (6)$$

where $[S_P(\omega)]$ is a diagonal matrix and its terms represent the spectral density functions of modal forces; $[H_\eta(\omega)]=diag[H_{\eta_j}(\omega)]$ denotes the frequency response function matrix of the structure; and $[H_\eta^*(\omega)]$ is its conjugate matrix. The mean-square response of the jth coordinate is given by

$$E[\eta_j^2(t)]=2\int_0^\infty S_{\eta_j}(\omega)d\omega\,. \qquad (7)$$

The correlation functions of external force $F_d(t)$ and actuator force $F_A(t)$ are defined as

$$R_{F_dF_A}(\tau)=E[F_d(t)F_A(t+\tau)]\,. \qquad (8)$$

A numerical magnitude of correlation between $F_d(t)$ and $F_A(t+\tau)$ can be determined by introducing the correlation coefficient, $\rho_{F_dF_A}$, defined as

$$\rho_{F_dF_A}=\frac{\sigma_{F_dF_A}}{\sigma_{F_d}\sigma_{F_A}}\,, \qquad (9)$$

where σ_{F_d} and σ_{F_A} represent the standard deviation of external random force $F_d(t)$ and actuator force $F_A(t)$ respectively. $\sigma_{F_dF_A}$ is the covariance of the external and actuator forces, which indicate the deviations of $F_d(t)$ and $F_A(t)$ from their centroid, and is given by [12]

$$\sigma_{F_dF_A}^2=E\left[F_dF_A\right]-\mu_{F_d}\mu_{F_A}\,, \qquad (10)$$

where μ_{F_d} and μ_{F_A} represent the mean value of external random force and the mean value of applied actuator force, respectively. Values of $\sigma_{F_dF_A}\cong 0$ indicate that the two signals tend not to vary together. As the units of external and actuator forces are different, the covariance $\sigma_{F_dF_A}$ should be normalized to remove the units of measurements. It should be noted that the values of $\rho_{F_dF_A}=\pm 1$ indicate that there is a perfect correlation, and $\rho_{F_dF_A}=0$ means that there is no correlation between the external and control forces.

3.1 State space form

Considering $\{x\} = \{\{\eta\}, \{\dot{\eta}\}\}^T$, the equation of motion in the state space form is given as

$$\{\dot{x}\} = [A]\{x\} + [B]\{\psi^a\} + \{f_d\},$$
$$\{\psi^s\} = \{y\} = [C]\{x\}, \tag{11}$$

where

$$[A] = \begin{bmatrix} [0] & [I] \\ [-\omega^2] & [-2\xi\omega] \end{bmatrix} \quad [B] = \begin{bmatrix} 0 \\ -[q]^T[K_{d\psi}^{sa}] \end{bmatrix}$$
$$[C] = [-[K_{\psi\psi}^{ss}]^{-1}[K_{\psi d}^{ss}][q] \quad [0]]$$
$$\{f_d\} = \{\{0\} \quad [q]^T\{F_d\}\}^T \tag{12}$$

3.2 Linear quadratic regulator (LQR)

Based on *LQR*, the feedback gain, K_{sc}, is chosen to minimize a quadratic cost function of the form

$$J = \frac{1}{2}\int_0^\infty \left(\{x\}^T[Q]\{x\} + \{u_c^T\}[R]\{u_c\}\right)dt, \tag{13}$$

where $[Q]$ is a symmetric semi-positive definite, and $[R]$ is a positive definite weighting matrix. Both are selected to provide suitable performance. The relative magnitudes of $[Q]$ and $[R]$ are selected to trade off on the requirements for minimizing vibration energy against the requirements for minimizing control voltage. In general, a larger $[Q]$ places a higher demand on control voltage, while a larger $[R]$ places more limits on the applied control force. In the full state control method, the actuating voltage is determined as

$$\{u_c\} = \{\psi^a\} = -[K_{sc}]\{x\}, \tag{14}$$

where $[K_{sc}]$ is the optimal feedback gain. For more details on optimal control, the book by Naidu [13] can be consulted. Substituting Eq. (14) into Eq. (11), the closed-loop state equation is obtained as

$$\{\dot{x}\} = ([A] - [B][K_{sc}])\{x\} + \{f_d\}, \tag{15}$$

and the frequency response function in state space form is determined as

$$H_\eta(j\omega) = \left(j\omega I - ([A] - [B][K_{sc}])\right)^{-1} \tag{16}$$

4. Numerical examples

4.1 Cross- ply configuration

A smart laminated beam with $[PS/(0/90/0)_s PA]$ (*PS* and *PA* stand for piezoelectric sensor and actuator layers, respectively) configuration with clamped-free boundary condition is considered.

Table 1. Material and geometric properties.

Property	Graphite/Epoxy	Piezoceramic	PVDF
E_1, GPa	98.0	71.4	4.67
E_2, GPa	6.78	71.4	-
4.80	3.48	24.8	2.66
P, KG/m^3	1380	7610	1610
D_{31}, m/V	-	$-200x10^{-12}$	$-20x10^{-12}$
E_{33}, F/m	-	$150x10^{-10}$	$1.05x10^{-10}$
Length, *L*, mm	300.0	25.0	25.0
Width, *b*, mm	30.0	25.0	25.0
Thickness, mm	0.2	0.50	0.0028

The material and geometric properties of composite lamina and the piezoceramic and Polyvinyliden Fluoride (PVDF) patches are provided in Table 1. The first three natural frequencies of this system are, 17.93 Hz, 105.98 Hz, and 276.07 Hz, respectively. The three natural frequencies are sufficiently separated to be considered independently. The beam is exposed to a random excitation applied at the tip and is approximated as Gaussian white noise with zero mean value, variance of 95.0 N^2, and standard deviation of 9.70 *N*. To suppress the vibration for the first two frequencies, the coefficients $[Q]$ and *R* corresponding to *LQR* are considered as $Q = 2\times10^9 I_{4\times4}$ and $R = 1.3$, respectively. The open-loop and closed-loop tip displacements in time domain are obtained, as shown in Fig. 1. As indicated earlier, applying the *LQR* control significantly suppresses the vibration response of the system.

The required applied control voltage on the actuator is also provided in Fig. 2. The variance of the actuator voltage is 3417 V^2, and its standard deviation and mean value are 58.5 V and 0.25 V, respectively. The correlation coefficient between the actuation voltage and the random excitation is $\rho_{F_d F_A} = 0.658$, which is sufficient for designing an active control system. It should be noted that for a deterministic sinusoidal external force, the correlation coefficient should be 0.998. The frequency response of the system is shown in Fig. 3, which illustrates that most of the power of the actuating signal is concentrated at the frequency close to the fundamental natural frequency of the system.

This result is expected, as the maximum deformation occurs at the fundamental natural frequency. Thus, most of the actuating energy supplied by the actuator is consumed at this frequency.

Random vibration analysis in time domain is very comprehensive. However, in various practical engineering applications, the input signal in time domain is not available and only the stochastic characteristic of the input random excitation is given. This gives rise to the need for an analysis based on the random properties of the signal, usually the power spectral density (PSD) function. To study the effect of structural configuration on random vibration control, a Gaussian white noise

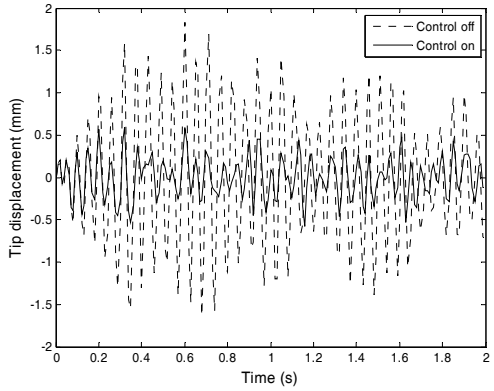

Fig. 1. Response of the smart laminated beam subject to white noise.

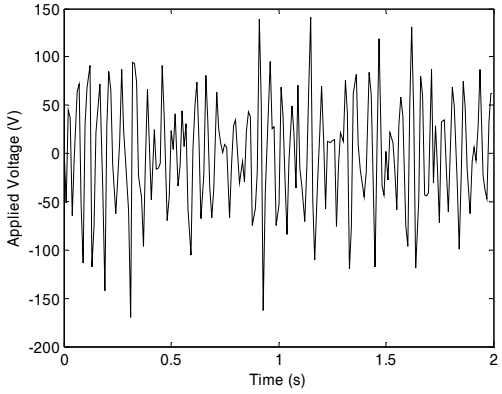

Fig. 2. Actuator voltage required to suppress the vibration.

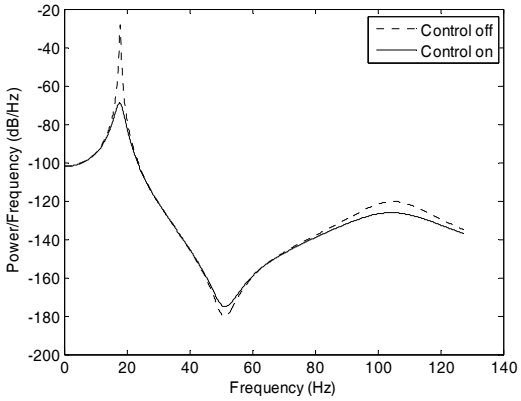

Fig. 3. PSD for smart laminated beam using control-on /off; the first two modes.

with a given $PSD_P = 40\,dB$ and zero mean value is considered, and the displacement response is also converted to decibel (dB), which is commonly used for *PSD* plots.

4.2 Effect of laminate configurations

The effect of laminate configuration on the PSD of the system response under a Gaussian white-noise random loading with a PSD of 40 dB is studied and is shown in Fig. 4.

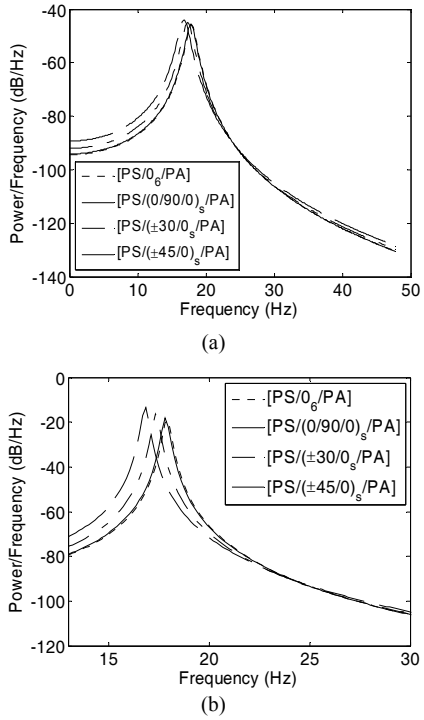

Fig. 4. Effect of laminate configuration on PSD of (a) closed-loop; (b) open-loop response.

The power consumption for smart systems with configurations of $[PS/(0/90/0)_s/PA]$ and $[PS/(0)_6/PA]$ is almost the same but is lower than that of smart systems with laminate configurations of $[PS/(\pm 30/0)_s/PA]$ and $[PS/(\pm 45/0)_s/PA]$. Moreover, the maximum amount of energy consumption for later configuration shifts to the left, which is due to the lower natural frequency for these laminates.

The effect of laminate configuration on the statistical properties of the structural-controlled response of the smart laminated beam under the same Gaussian white-noise excitation is provided in Table 2. The table shows that the laminate configuration of $[PS/(\pm 45/0)_s/PA]$ has the highest value for the mean, standard deviation, and variance followed by the configuration of $[PS/(\pm 30/0)_s/PA]$. The two other configurations $[PS/(0/90/0)_s/PA]$ and $[PS/(0)_6/PA]$ are almost the same and have lower values compared with the other two cases.

An important observation in random analysis is the correlation coefficient between the actuation voltage and the random excitation.

The correlation coefficient, $\rho_{F_d F_A}$, for different configurations is given in Table 3. For softer configuration, that is, $[PS/(\pm 45/0)_s/PA]$, the correlation coefficient is higher than that for harder configurations. It should be noted that for a deterministic sinusoidal external force, the correlation coefficient should be 0.998.

4.3 Random vibration for aerospace applications

The narrow-band process, which simulates the operating

Table 2. Effect of laminate configurations on the statistical properties of the tip displacement of the smart beam for closed-loop control.

	Statistical properties of tip displacement		
Laminate configuration	μ_{tip}, mm	σ_{tip}, mm	σ_{tip}^2, mm^2
$[PS/(0)_6/PA]$	0.0006	0.240	0.058
$[PS/(\pm30)/0)_s/PA]$	0.0007	0.248	0.0616
$[PS/(\pm45)/0)_s/PA]$	0.0008	0.257	0.066
$[PS/(0/90/0)_s/PA]$	0.0006	0.242	0.058

Table 3. The correlation coefficient, $\rho_{F_d F_A}$ for different laminate configurations.

Laminate configuration	Correlation coefficient, $\rho_{F_d F_A}$
$[PS/(0/90/0)_s/PA]$	0.658
$[PS/(\pm30)/0)_s/PA]$	0.671
$[PS/(\pm45)/0)_s/PA]$	0.692

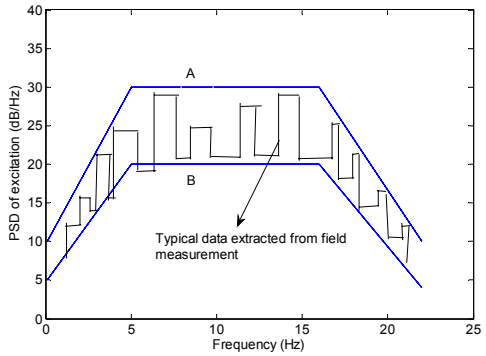

(a)

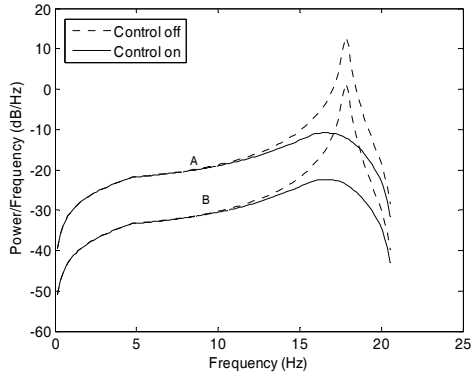

(b)

Fig. 5. (a) PSD of random vibration; (b) response under aerospace random input.

environments, is of great importance in the design of aerospace structures. A typical example of the vibration data extracted from the vibration measurement of aircraft structures is shown in Fig. 5(a) [14]. However, such a spectrum is too complicated to be used as a test spectrum. Thus, the envelope of the spectrum is considered.

The laminate configuration is assumed to be $[PS/(0/90/0)_s/PA]$. The upper, A, and lower, B, envelopes of the PSD are given in Fig. 2(a). For the conservative test, that is, the test is more severe than the environment, curve A can be used to overestimate the environment, whereas curve B can be considered for underestimated experiments. The frequency range is considered from 1 to 20 Hz to cover the frequencies below and those slightly beyond the fundamental frequencies of the system. The PSDs of the response of the smart beam subjected to both upper envelope A and lower envelope B are shown in Fig. 5(b). The open-loop and closed loop responses are provided to demonstrate the performance of the controlled system for typical and practical random loading conditions.

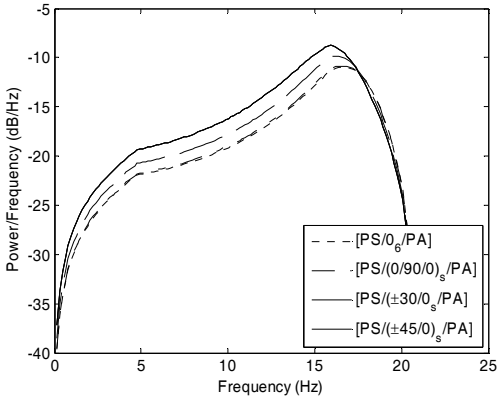

(a)

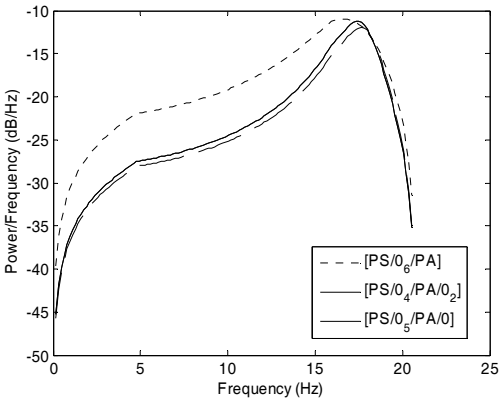

(b)

Fig. 6. Effect of (a) laminate configuration and (b) actuator location through the thickness on the response due to envelope A.

For both envelopes, the power is well distributed through the frequency range. However, as it is expected that the peak value will occur around the natural frequency of the system, the configuration of $[PS/(\pm45/0)_s/PA]$ has the highest peak level that occurs at lower frequencies compared with other configurations. The configurations with higher stuffiness, $[PS/(0/90/0)_s/PA]$ and $[PS/(0)_6/PA]$, provide lower levels of power consumption. These conclusions are similar to the corresponding results obtained for the smart system subjected to white noise.

The important feature is that for all cases, the PSD is evenly distributed in the frequency range. Moreover, the peak that occurs at the fundamental natural frequency is effectively suppressed when the control is on.

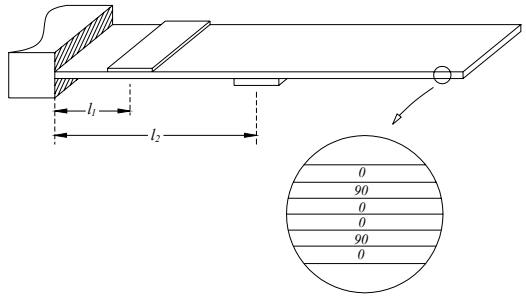

Fig. 7. Smart laminated beam with uncollocated sensor/actuator pairs.

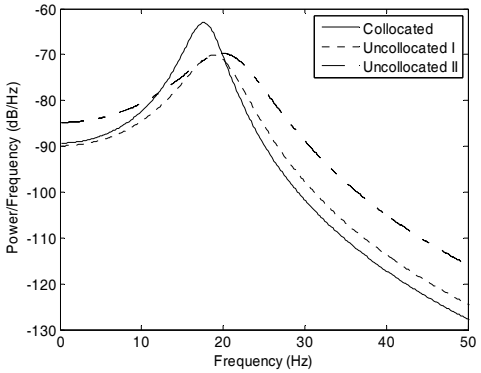

Fig. 8. Effect of collocated and uncollocated PZT pair on the response of the smart beam.

4.4 Effect of actuator location

The effect of actuator location on the power spectrum of the smart system subjected to envelope A is also presented in Fig. 6(b). Three different locations, which are chosen through the thickness, are considered: $[PS/(0)_6/PA]$, $[PS/0_5/PA/0]$, and $[PS/0_4/PA/0_2]$. When the actuator is located far from the mid-point, the PSD is lower, whereas when the actuator is located inside the laminate, power consumption is higher. This is due to the moment effect of actuator when located far from the mid-point.

4.5 Collocation effect of sensor/actuator

The effect of collocated and uncollocated sensor/actuator pairs on optimal vibration control is also investigated, and results are presented through the following example. Two cases of uncollocated sensor/actuator pairs are considered, as shown in Fig. 7. In case I, the sensor is mounted on the top surface at $l_1 = 3cm$ from the fixed end, while the actuator is bonded on bottom surface at $l_2 = 6cm$ from the fixed end. In case II, the actuator is bonded at $l_2 = 8cm$ from the fixed end on the bottom surface, while the location of sensor remains the same as that in case I.

Fig. 8 shows that for collocated sensor/actuator pairs, the peak of power is higher than the uncollocated pairs and occurs at the lower frequency. As the actuator shifts away from the sensor location, the peak of power occurs at higher frequency and becomes more distributed through all the frequencies in the domain.

5. Conclusion

A parametric study is conducted to investigate the effects of laminate configurations and smart elements on the vibration response of smart laminated beams under random loading. A control algorithm utilizing linear quadratic regulator and layer-wise displacement finite element formulation is also utilized to determine the controlled responses under random excitations.

The effects of laminate configuration and smart element location on the vibration response of the system for the closed-loop system are also investigated.

The configuration of $[PS/(\pm 45/0)_s/PA]$ shows the highest value for the mean, standard deviation, and variance compared with the other configuration under study. To demonstrate the correlation between the input random force and the applied actuator voltage, the correlation coefficients for different laminate configurations are provided. For softer configurations, that is, $[PS/(\pm 45/0)_s/PA]$, the correlation coefficient is higher that that for harder configurations.

The study deals with the frequency domain by considering narrow-band processes, particularly for aerospace applications. The PSDs of the displacement responses for different laminate configurations and smart element locations of the system subjected to a known input power spectral density of the excitation are computed. The configuration of $[PS/(\pm 45/0)_s/PA]$ has the highest peak level, which occurs at lower frequencies, compared with other configurations. Furthermore, when the actuator is located far from the mid-point, the PSD is lower, whereas when the actuator is located inside the laminate, power consumption is higher. The study on the effects of sensor/actuator collocation pairs on optimal vibration control reveals that as the actuator shifts away from the sensor location, the peak of power occurs at higher frequency and becomes more distributed through all the frequencies in the domain.

Acknowledgment

This work was partially supported by the Sharif University of Technology, International Campus on Kish Island under Grant number 01/9408. The author would like to acknowledge the interesting discussion provided by R. Sedaghati and R. Ganesan of Concordia University.

Nomenclature

$[K]$: Stiffness matrix
$\{\psi\}$: Electrical potential
$[M]$: Mass matrix
$\{d\}$: Displacement vector
$[S]$: Power spectral density

References

[1] D. M. Frangopol and S. Recek, Reliability of Reinforced Composite Laminated Plates, *Probab. Eng. Mech.,* 18 (2003)

119-137.
[2] L. Librescu and I. Elishakoff, Response of Laminated Plates to Non-stationary Random Excitation, *Struct. Saf.,* 6 (1998) 99-113.
[3] G. Cederbaum, L. Librescu and I. Elishakoff, Random Vibration of Laminated Plates Modeled Within the First-order Shear Deformation Theory, *Compos. Struct.,* 12 (1989) 97-111.
[4] J. Kang and R. S. Harichandran, Random Vibration of Laminated FRP Plates with Material Nonlinearity using Higher-order Shear Theory, *J. Eng. Mech.,* 125 (9) (1999) 1081-1088.
[5] P., Dash, B.N., Singh, Nonlinear free vibration of piezoelectric laminated composite plate, *Finite Elem. Anal. Des.,* 45 (10) (2009) 686-694.
[6] D. H. Robbins and J. N. Reddy, Analysis of piezoelectrically actuated beams using a layer-wise displacement theory, *Compos.. Struct.,* 41 (2) (1991) 265-279.
[7] A. Zabihollah, R. Sedagahti and R. Ganesan, Active vibration suppression of smart laminated beams using layer-wise theory and optimal control strategy, *Smart Mater. Struct.,* 16 (2007) 1-12.
[8] S. Narayanana and V. Balamurugan, Finite Element Modeling of Piezo-laminated Smart Structures or Active Vibration Control with Distributed Sensors and Actuators, *J. Sound Vib.,* 262 (2003) 529-562.
[9] I. Bruant, G. Coffigal, F. Lene and M.Verge, A methodology for determination of piezoelectric actuator and sensor location on beam structures, *J. Sound Vib.,* 243 (5) (2001) 861-882.
[10] C. M. A. Vasques and J. D. Rodrigues, Active vibration control of smart piezoelectric beams: Comparison of classical and optimal feedback control strategies, *Comput. Struct.,* 84 (22-23) (2006) 1402-1414.
[11] M. Levent, Integration of active vibration control methods with finite element models of smart laminated composite structures, *Compos. Struct.,* 92 (2010) 1651-1663.
[12] C. Y. Yang, *Random Vibration of Structures*, John Wiley and Sons Inc., New York, (1986).
[13] D. Subbaram Naidu, *Optimal Control Systems*, CRC Press, USA, (2003).
[14] R. H. Lyon, *Random Noise and Vibration in Space Vehicles*, Shock and Vibration Information Center, U.S. Dept. of Defense, Washington, (1967).

Appendix : Element matrices for smart laminated beams

Stiffness and mass matrices of smart laminated beams based on layer-wise displacement theory are given by

$$[K_{dd}]=\begin{bmatrix}[K^{11}] & [K^{12}]\\ [K^{12}]^T & [K^{22}]\end{bmatrix},\ [M_{dd}]=\begin{bmatrix}[M^{11}] & [0]\\ [0] & [M^{22}]\end{bmatrix}.$$

The coefficients of the element matrices are given by

$$[K_{d\psi}]=\int_0^l\left([E_{31}][S][S_{,x}]\right)dx,\ [K_{\psi d}]=[K_{d\psi}]^T$$

$$[K_{\psi\psi}]=\int_0^l\left([G_{33}][S][S]\right)dx$$

$$[K_{dd}^{11}]=\int_0^l\left([A_{11}][S_{,x}][S_{,x}]+[D_{55}][S][S]\right)dx$$

$$[K_{dd}^{12}]=\int_0^l\left([B_{13}][S_{,x}][S]+[D_{55}][S_{,x}][S]\right)dx\quad [K_{dd}^{21}]=[K_{dd}^{12}]^T$$

$$[K_{dd}^{22}]=\int_0^l\left([A_{55}][S_{,x}][S_{,x}]+[D_{33}][S][S]\right)dx$$

$$\rho^{2-IJ}=\sum_{k=1}^{N_p}\int_{-h/2}^{h/2}b\rho^k dz$$

$$[M_{dd}^{11}]=\int_0^l\left([\rho^1][S][S]\right)dx$$

$$[M_{dd}^{22}]=\int_0^l\left([\rho^2][S][S]\right)dx$$

$$E_{31}^{IJ}=\sum_{k=1}^{N_p}\left[\int_{z_k}^{z_{k+1}}b\bar{C}_{13}^k d_{31}\Phi^I\frac{\partial\Phi^J}{\partial z}dz\right]$$

$$G_{33}^{IJ}=\sum_{k=1}^{N_p}\left[\int_{z_k}^{z_{k+1}}b\bar{g}_{33}\frac{\partial\Phi^I}{\partial z}\frac{\partial\Phi^J}{\partial z}dz\right]$$

$$A_{11}^{IJ}=\sum_{k=1}^{N_p}\left[\int_{z_k}^{z_{k+1}}b\bar{C}_{11}^k\Phi^I\Phi^J dz\right]\quad A_{55}^{IJ}=\sum_{k=1}^{p\,p}\left[\int_{z_k}^{z_{k+1}}b\bar{C}_{55}^k\Phi^I\Phi^J dz\right]$$

$$B_{13}^{IJ}=\sum_{k=1}^{N_p}\left[\int_{z_k}^{z_{k+1}}b\bar{C}_{13}^k\frac{\partial\Phi^I}{\partial z}\Phi^J dz\right]\quad B_{55}^{IJ}=\sum_{k=1}^{N_p}\left[\int_{z_k}^{z_{k+1}}b\bar{C}_{55}^k\frac{\partial\Phi^I}{\partial z}\Phi^J dz\right]$$

$$C_{13}^{IJ}=\sum_{k=1}^{N_p}\left[\int_{z_k}^{z_{k+1}}b\bar{C}_{13}^k\Phi^I\frac{\partial\Phi^J}{\partial z}dz\right]\quad C_{55}^{IJ}=\sum_{k=1}^{N_p}\left[\int_{z_k}^{z_{k+1}}b\bar{C}_{55}^k\Phi^I\frac{\partial\Phi^J}{\partial z}dz\right]$$

A. Zabihollah received his Ph.D. in mechanical engineering from Concordia University, Montreal, Canada in 2007. He is the author of over 25 publications on smart structures, vibration suppression, and design optimization. Dr. Zabihollah is currently working at the international campus of Sharif University of Technology on Kish Island.